Journal of Materiomics 9 (2023) 492–501

Contents lists available at ScienceDirect

Journal of Materiomics

journal homepage: www.journals.elsevier.com/journal-of-materiomics/

Building the conformal protection of VB-group VS_2 laminated heterostructure based on biomass-derived carbon for excellent broadband electromagnetic waves absorption

Honghan Wang [a, b], Huibin Zhang [a], Junye Cheng [c, *], Tingting Liu [d], Deqing Zhang [a, **], Guangping Zheng [e], Shangru Zhai [b, ***], Maosheng Cao [d, ****]

[a] School of Materials Science and Engineering, Qiqihar University, Qiqihar, 161006, China
[b] Liaoning Key Lab of Lignocellulose Chemistry and BioMaterials, Liaoning Collaborative Innovation Center for Lignocellulosic Biorefinery, College of Light Industry and Chemical Engineering, Dalian Polytechnic University, Dalian, 116034, China
[c] Department of Materials Science, Shenzhen MSU-BIT University, Shenzhen, Guangdong Province, 517182, China
[d] School of Materials Science and Engineering, Beijing Institute of Technology, Beijing, 100081, China
[e] Department of Mechanical Engineering, Hong Kong Polytechnic University, Hung Hom, Kowloon, Hong Kong, China

ARTICLE INFO

Article history:
Received 9 October 2022
Received in revised form
28 November 2022
Accepted 10 December 2022
Available online 19 January 2023

Keywords:
VS_2/GDC hybrids
Multi-interface heterostructures
Broadband absorption
Environmental stability

ABSTRACT

Although VB-Group transition metal disulfides (TMDs) VS_2 nanomaterials with specific electronic properties and multiphase microstructures have shown fascinating potential in the field of electromagnetic wave (EMW) absorption, the efficient utilization of VS_2 is limited by the technical bottleneck of its narrow effective absorption bandwidth (EAB) which is attributed to environmental instability and a deficient electromagnetic (EM) loss mechanism. In order to fully exploit the maximal utilization values of VS_2 nanomaterials for EMW absorption through mitigating the chemical instability and optimizing the EM parameters, biomass-based glucose derived carbon (GDC) like sugar-coating has been decorated on the surface of stacked VS_2 nanosheets *via* a facile hydrothermal method, followed by high-temperature carbonization. As a result, the modulation of doping amount of glucose injection solution (Glucose) could effectively manipulate the encapsulation degree of GDC coating on VS_2 nanosheets, further implementing the EM response mechanisms of the VS_2/GDC hybrids (coupling effect of conductive loss, interfacial polarization, relaxation, dipole polarization, defect engineering and multiple reflections and absorptions) through regulating the conductivity and constructing multi-interface heterostructures, as reflected by the enhanced EMW absorption performance to a great extent. The minimum reflection loss (R_{min}) of VS_2/GDC hybrids could reach −52.8 dB with a thickness of 2.7 mm at 12.2 GHz. Surprisingly, compared with pristine VS_2, the EAB of the VS_2/GDC hybrids increased from 2.0 to 5.7 GHz, while their environmental stability was effectively enhanced by virtue of GDC doping. Obviously, this work provides a promising candidate to realize frequency band tunability of EMW absorbers with exceptional performance and environmental stability.

1. Introduction

The hazards to human being from prolonged exposure to electromagnetic (EM) irradiation resulting from the extensive utilization of EM devices are incalculable, since the interaction between redundant electromagnetic waves (EMWs) and human body which is attributed to the fact that EM energy conduction has a negative effect on human body function, and also interferes with the normal operation of electronic equipment. Thus, the purification of excessive EM energy is essential, considering the safety and environmental-friendliness of the human social environment [1–3]. Recently, the VIB-group two-dimensional (2D) transition metal disulfides (TMDs) such as MoS_2 [4–6] and WS_2 [7,8] are of much interest for their applications in EMW absorption due to their

* Corresponding authors.
** Corresponding author.
*** Corresponding authors.
**** Corresponding author.
E-mail addresses: chengjunye@smbu.edu.cn (J. Cheng), 00582@qqhru.edu.cn (D. Zhang), zhaisr@dlpu.edu.cn (S. Zhai), caomaosheng@bit.edu.cn (M. Cao).
Peer review under responsibility of The Chinese Ceramic Society.

https://doi.org/10.1016/j.jmat.2022.12.003

peculiar electronic structures, large specific surface area, multiphase microstructures with the coexistence of 1T, 2H and 3R phases [9,10] and abundant active sites. With the rapid development of electronic technology and increasing demand on EMW absorption, the VIB-group TMDs have exhibited some shackles in practical applications, such as the narrow effective absorption bandwidth (EAB) that is caused by the finite active sites located only at the edges of their microstructures, and the difficulty in achieving appropriate impedance matching because of the limitations of their energy band structures [7,8]. Therefore, extensive efforts have been devoted to the design of new-generation EMW absorbers with indispensable capability of EM energy transduction.

The VB-group TMDs VS_2 nanomaterials are novel EMW absorbing materials, which can be modulated to become either semiconductors or metallic materials through altering their crystal structures or the number of stacked layers. Particularly, VS_2 nanomaterials can be prepared with well-tuned synthesis routes to exhibit electrochemical active sites at the edges of their microstructures and inside their stacked layers, which could break the aforementioned bottleneck of VIB-group TMDs (such as WS_2 or MoS_2) for EMW absorption applications [11]. Zhang et al. have synthesized the coaxial stacking VS_2 nanosheets *via* a facile one-step hydrothermal route, which have the minimum reflection loss (R_{min}) as low as −57.0 dB at 4 GHz [12], while other reported TMDs have to incorporate other materials to construct multicomponent heterostructures with multiple loss mechanisms to achieve such exceptional EMW absorption performance. In order to further enhance the EMW absorption performance of VS_2 nanosheets which exhibit narrow bandwidth and chemical instability under an oxidation environment, it is an effective strategy that multicomponents could be introduced into the VS_2 nanosheets to construct multi-interface heterostructures and protective layers of the nanosheets [13–16].

Carbon nanomaterials, such as graphene and CNTs, have become typical representatives of EMW absorbers operated in the high-frequency range due to their high conductivity, nanostructures with large specific surface area and abundant defects as well as the facilely tuned dielectric properties and impedance matching [17–20]. In most cases, exploiting the complementarity of dielectric-loss materials and conductive carbon-based materials is an effective strategy to design EM attenuation systems with high performance, which can further facilitate the effective absorption of EMWs by defect engineering and 3D conductive networks in the systems [21]. The multiple loss mechanisms, such as multiple internal reflections and scattering, dipole polarization caused by abundant functional groups and defects, as well as interfacial polarization presented at multi-interface heterostructures, could be essential for the attenuation of EM energy [22]. Although the carbon nanomaterials as represented by graphene and CNTs are expected to regulate the EM parameters of VS_2 nanomaterials by virtue of their well-known outstanding environmental stability and conductive properties, they cannot form ideal protective layers with porous or reticular structures onto the VS_2 nanomaterials, which may not fully encapsule VS_2 nanomaterials to improve their environmental and chemical stability. Being alternatives to conventional carbon-based materials, the biomass derived carbon-based materials adhering to the concept of green chemistry are considered to be promising resources in facilely synthesizing environmental-friendly and efficient EMW absorbers [23,24]. In addition to the advantages of conventional carbon-based materials such as low density, high conductivity and high dielectric loss, they can be used as natural templates for the preparation of EMW absorbers with low cost, simple preparation process and preeminent EMW absorption performance [25–27]. Furthermore, some laminated carbon materials, which are derived mostly from biomass, can be uniformly coated on the surface of VS_2 nanomaterials by combining solution coating with high-temperature carbonization. Dong *et al.* successfully prepared the core-shell SiCw@C heterostructures with thickness-dependent EMW absorption in X-band and Ku-band by combining a hydrothermal synthesis route and carbonization processes, with glucose being the carbon precursor [28]. The R_{min} value was as low as −61.2 dB with EAB located in the whole X-band and Ku-band, which was attributed to the dipole polarization, interfacial polarization, relaxation polarization and the well-matched impedance in the systems. The coating layer of carbon materials not only enhanced the environmental and chemical stability of the EMW absorbing materials, but also constructed a large number of multi-interface heterostructures, leading to a promising candidate for the development of efficient and stable EMW absorbing materials.

In this work, VS_2/glucose-derived carbon (GDC) hybrids were successfully prepared *via* a simple hydrothermal method followed by high-temperature carbonization, using glucose as carbon precursor. The distinctive microstructures, morphological characteristics and prominent EMW absorption performance of VS_2/GDC hybrids, which could be optimized by the content of GDC doping, has been systematically investigated. The EMW absorption mechanisms are analyzed based on the EM properties, impedance matching and attenuation constant of the VS_2/GDC hybrids. It is revealed that the microstructure of VS_2 nanomaterials can be tuned with the assistance of GDC encapsulation and the VS_2/GDC hybrids show superior EMW absorption performances with efficient EM attenuation, wide EAB at a small thickness and a lower content of glucose. Undoubtedly, this work could open a new avenue for the development of TMDs/biomass-based EMW absorbing materials with low cost, environmental friendliness and excellent EMW absorption performance.

2. Experimental

2.1. Materials

Ammonium metavanadate (NH_4VO_3) was purchased from China Pharmaceutical Shanghai Chemical Reagent Company. Thioacetamide (CH_3CSNH_2) was purchased from Tianjin Guangfu Fine Co. Ltd.. Polyvinylpyrrolidone (PVP) was purchased from Xianshuigu Industrial Park, Jinan District, Tianjin. Ammonia ($NH_3 \cdot H_2O$) was purchased from Tianjin Kaitong Chemical Reagent Co. Ltd. The aforementioned raw materials were of analytical grade and employed without further purification. Glucose injection solution (Glucose) was purchased from Henan Kelun Pharmaceutical Co. Ltd. (50%, in mass), which could be used directly in experiments.

2.2. Synthesis of VS_2 nanosheets

Firstly, 1.310 4 g of NH_4VO_3, 15.288 g of NH_3H_2O, 4.205 6 g of CH_3CSNH_2 and 2.800 g of PVP were dissolved in 84 mL of deionized water under continuously stirring for 1 h to obtain a homogeneous solution. Then, the solution was transferred into a 140 mL polytetrafluoroethylene (PTFE) reactor and sealed in a stainless-steel hydrothermal vessel that was heated at 190 °C for 12 h. After the reaction, the reactor was cooled to room temperature, and the precipitate was collected after centrifugation, washing by deionized water and absolute ethanol for several times, and drying in vacuum at 60 °C for 12 h. The obtained samples were denoted as VS_2 nanosheets.

2.3. Synthesis of GDC

The evenly stirred solution (69 mL of deionized water and 15 mL

of Glucose was transferred into a stainless steel hydrothermal vessel with a 140 mL PTFE reactor, which was heated at 190 °C for 12 h. After the reaction, the reactor was cooled to room temperature, the precipitate was collected after centrifugation, washing by deionized water and absolute ethanol for several times, and drying in vacuum at 60 °C for 12 h. The dried product was transferred into a tube furnace and heated at 700 °C for 2 h (with a heating rate of 5 °C/min) under nitrogen atmosphere. Finally, the product was cooled to room temperature, which was denoted as GDC-700 °C.

2.4. Synthesis of the VS_2/GDC hybrids

The as-prepared VS_2 (1 g in mass), 69 mL of deionized water and 15 mL of Glucose were stirred evenly. Then, the mixture was transferred into a 140 mL polytetrafluoroethylene (PTFE) reactor, which was sealed in a stainless-steel hydrothermal vessel for the reaction to occur at 190 °C for 12 h. After the reaction, the reactor was cooled to room temperature, and the precipitate was collected after centrifugation, washing by deionized water and absolute ethanol for several times, and drying in vacuum at 60 °C for 12 h. The dried product was transferred into a tube furnace and heated to 700 °C under nitrogen atmosphere with a heating rate of 5 °C/min. The reaction lasted for 2 h and the reactor was then cooled to room temperature. The obtained sample was denoted as VS_2/15GDC-700 °C. The total volume of the added deionized water and Glucose was 84 mL, and the volume of Glucose was 10 mL and 20 mL, corresponding to the samples denoted as VS_2/10GDC-700 °C and VS_2/20GDC-700 °C, respectively.

2.5. Characterization

The X-ray diffraction (XRD) patterns were recorded using Bruker-AXS D8 X-ray diffractometer with Cu K_α radiation ($\lambda = 0.1546$ nm). The XPS analysis was carried out on X-ray photoelectron spectrometer (ESCALAB250Xi, Thermofisher Co). The morphology and crystal structure of the as-synthesized products were characterized by scanning electron microscope (SEM, S-4300; Hitachi) with an accelerating voltage of 20 kV and transmission electron microscopy (TEM, Hitachi, H-7650). The electromagnetic properties of the samples were determined by the coaxial method with a vector network analyzer (VNA, MS-200644A Anritsu) in the frequency range of 2–18 GHz. The samples containing 60% (in mass) paraffin wax were prepared.

3. Results and discussion

The preparation process of VS_2/GDC hybrids is schematically illustrated in Fig. 1, which includes the pre-preparation of coaxial stacked VS_2 nanosheets and the subsequent synthesis of VS_2/GDC hybrids. Briefly, NH_4VO_3 and CH_3CSNH_2 provide the sources of V and S elements for the preparation of coaxial stacked VS_2 nanosheets in an alkaline environment by $NH_3{\cdot}H_2O$ and assisted surfactant PVP. V^{4+} and S^{2-} are combined by covalent bonds to form multilayer stacked hexagonal nanosheets with varying sizes as peeled by $NH_3{\cdot}H_2O$, which are attributed to NH_3 and NH^{4+} decomposed from $NH_3{\cdot}H_2O$ to weaken the agglomeration of VS_2 nanosheets. Subsequently, the Glucose could be easily carbonized to the carbon shell like sugar coating under nitrogen atmosphere and form the VS_2/GDC multi-interface heterostructures, which is conducive to providing a stable chemical environment for VS_2 and enhancing the EMW attenuation through effective multiple loss mechanisms such as conductive loss, dipole polarization, interface polarization, multiple reflections and scattering. As a result, the 3D conductive network can be controlled by the amount of Glucose doping, carbonization temperature and carbonization time, which could promote the strong coupling effect between impedance matching and attenuation constants.

The XRD patterns of VS_2, GDC-700 °C, VS_2/15GDC-700 °C are presented to demonstrate the phase evolutions of the hybrids after being annealed at 700 °C for 2 h under nitrogen atmosphere, as shown in Fig. 2a. The diffraction patterns of VS_2 have four obvious broad peaks located at 15.0°, 32.3°, 45.1°, 57.0°, corresponding to the (001), (100), (012) and (110) crystal planes of VS_2 nanomaterials (PDF#89-1640, P-3m1-164 lattice group), respectively [12]. There are several weak impurity peaks as observed in the patterns, confirming that the VS_2 nanomaterials have good crystallinity. After the pyrolysis of glucose at 700 °C, the peak located at 20.0° can be well indexed to (002) plane of typical incompletely carbonized carbon which not only preserves the carbon skeleton but also introduces a moderate amount of carbon into the EMW absorption system to regulate the impedance matching. The peaks in the XRD patterns of VS_2/15GDC-700 °C are similar to those of VS_2 except the (011) peak. Since the TMD hybrid contains a large number of 1T phase, the shifts of peaks in the XRD patterns of VS_2/15GDC-700 °C are due to the transition from the 1T phase to the 2H phase of VS_2 [29]. Unfortunately, the peak of carbon is not visible in the XRD patterns of VS_2/15GDC-700 °C, which is ascribed to the relatively low carbon contents that can ensure a suitable impedance matching for VS_2/15GDC-700 °C. As shown in Fig. 2b, combined with Raman spectra of VS_2/15GDC-700 °C, we can determine the existence of GDC and its graphitization degree, which can affect the micromorphology of coaxial stacked VS_2 nanosheets fully encapsulated by GDC, enhancing the EMW multiple scattering and reflection.

To further demonstrate the formation of effective multi-interface heterostructures between VS_2 and GDC, the surface chemical compositions and electronic state of each element of VS_2/15GDC-700 °C are determined by XPS analysis. As shown in Fig. 2c, the survey spectra of VS_2/15GDC-700 °C indicate different chemical environments of constituent elements (S, C, V, O) observed at 163.4, 285.8, 516.7, 530.6 eV, respectively. The oxidation state of V is characterized in Fig. 2d. The coexistence of V $2p_{3/2}$ and V $2p_{1/2}$ in the VS_2 crystal is evident by the distinctive main peaks located at 516.1 and 523.5 eV. In Fig. 2e, the S 2*p* spectrum exhibits two contributions (S $2p_{3/2}$ and S $2p_{1/2}$). The S–O peak located at a lower binding energy is attributed to the oxidized surface of VS_2, which also confirms the presence of O element. Especially, the ratio of S–O peak area of VS_2/15GDC-700 °C is significantly less than that of untreated VS_2 (Fig. S1), demonstrating that the fully encapsulated GDC provides a stable chemical environment for the system through conformal protection of VS_2. The C 1*s* spectrum of VS_2/15GDC-700 °C shown in Fig. 2f is mainly attributed to glucose treated by carbonation at 700 °C, where the peak at 284.3 eV could correspond to sp^3-hybridized C (C–C). The XPS results strongly suggest that VS_2 coexists with GDC within the EMW absorbing materials after the pyrolysis reaction, effectively forming a heterostructure of VS_2/GDC.

The microstructure and morphology of VS_2 nanosheets and VS_2/15GDC-700 °C are further analyzed by SEM and TEM, as shown in Fig. 3. Fig. 3a-b indicates that VS_2 are composed of hexagonal nanosheets with different sizes, and the averaged diameter of VS_2 nanosheets is about 1 μm. The rough surface of VS_2 nanosheets has different degrees of protrusion, which is conducive to their combination with GDC. A large number of defects carried by VS_2 nanosheets provide multi-polarization relaxation centers for EM attenuation, effectively improving the dielectric loss. The microstructure of VS_2 nanosheets consists of 1T phase (green circles) and 2H phase (yellow triangles), which can be associated with Fig. 3c. The multiphase (1T and 2H) VS_2 nanosheets prepared by adjusting the band structure activates the active sites inside the stacked

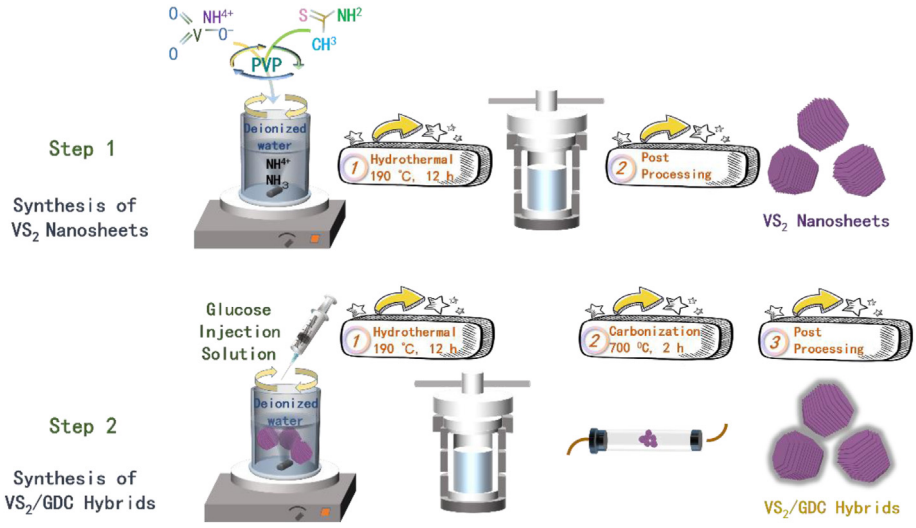

Fig. 1. Schematic illustration of the growth of VS_2 nanosheets and VS_2/GDC hybrids.

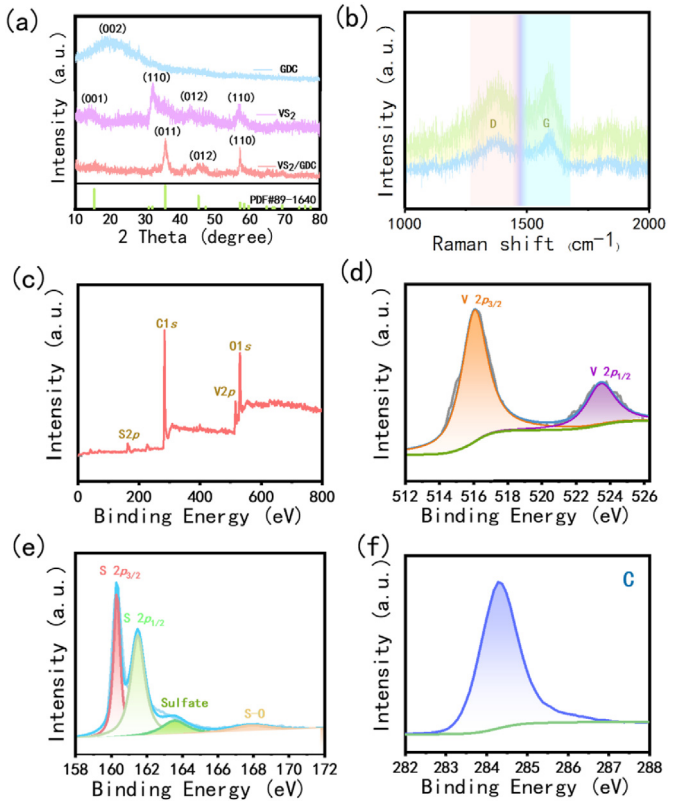

Fig. 2. (a) XRD and (b) Raman patterns of VS_2, GDC and VS_2/GDC hybrids; (c) XPS wide scan (survey) and high-resolution narrow scans on (d) V, (e) S and (f) C in VS_2/GDC hybrids.

layers besides the edges, which can serve as the center of polarization to promote dipole polarization. Furthermore, the intervention of a large number of 1T phases effectively adjusts the conductivity to obtain a suitable impedance matching. Fig. 3d-e shows that with the carbonization of Glucose, the carbon layers with different thicknesses are coated on the surface of VS_2 nanosheets, forming the sugar-like coating which can provide a stable chemical environment for VS_2, and the tightly packed carbon layers could prevent VS_2 nanosheets from being oxidized. It is suggested that VS_2 nanosheets fully encapsulated by GDC maintain the stable original coaxially stacked micromorphology of VS_2 nanosheets to a large extent while also exhibiting irregular edges and a certain thickness of GDC coating, which proves that the interlayer structure and edges of VS_2 nanosheets are in gapless contact with GDC and the multi-interface heterostructures are constructed. The incident EMWs are reflected and absorbed for multiple times between the layers of coaxially stacked VS_2 nanosheets, which contributes to the improvement of the attenuation constant.

In general, the EMW absorption performance can be evaluated by reflection loss (R), according to the transmit-line theory, which can be expressed by the following equations [30–32]:

$$R_L = 20 \lg \frac{|Z_{in} - Z_0|}{|Z_{in} + Z_0|}, \quad (1)$$

$$Z_{in} = Z_0 \sqrt{\frac{\mu_r}{\varepsilon_r}} \tan h \left[j \left(\frac{2\pi f d}{c} \right) \sqrt{\mu_r \varepsilon_r} \right], \quad (2)$$

where Z_{in} is the input impedance of the absorber, Z_0 is the impedance of free space, ε_r is the complex permeability, μ_r is the permittivity, f represents the EMW frequency, d is the thickness of the absorber, c is the velocity of light in free space (3×10^8 m/s). Obviously, the EM parameters ε_r ($\varepsilon_r = \varepsilon' - j\varepsilon''$) and μ_r ($\mu_r = \mu' - j\mu''$) are the main factors in evaluating the EMW absorption performance. To obtain the EM parameters for all samples, we tested the samples containing 60% (in mass) paraffin wax by using an Anritsu MS4644A vector network analyzer in the frequency range of 2.0–18.0 GHz. For non-magnetic materials such as VS_2 and GDC, μ' and μ'' are 1 and 0, respectively, meaning that the negligible magnetic loss does not play a dominant role in the EMW absorbing system. Since the real part (ϵ') of the relative complex permittivity represents the electric energy storage, while the imaginary part (ϵ'') is associated with the capacity of electric energy loss, for the dielectric-based absorbers, the dielectric loss tangent $\tan\delta_\varepsilon$ ($\tan\delta_\varepsilon = \varepsilon''/\varepsilon'$) relates to the degree of dielectric loss, and ε_r is explained by the Debye theory [33–35]:

$$\varepsilon_r = \varepsilon' - j\varepsilon' = \varepsilon_\infty + \frac{\varepsilon_s - \varepsilon_\infty}{1 + j2\pi f\tau}, \quad (3)$$

where ϵ' and ϵ'' can be expressed by the following equations:

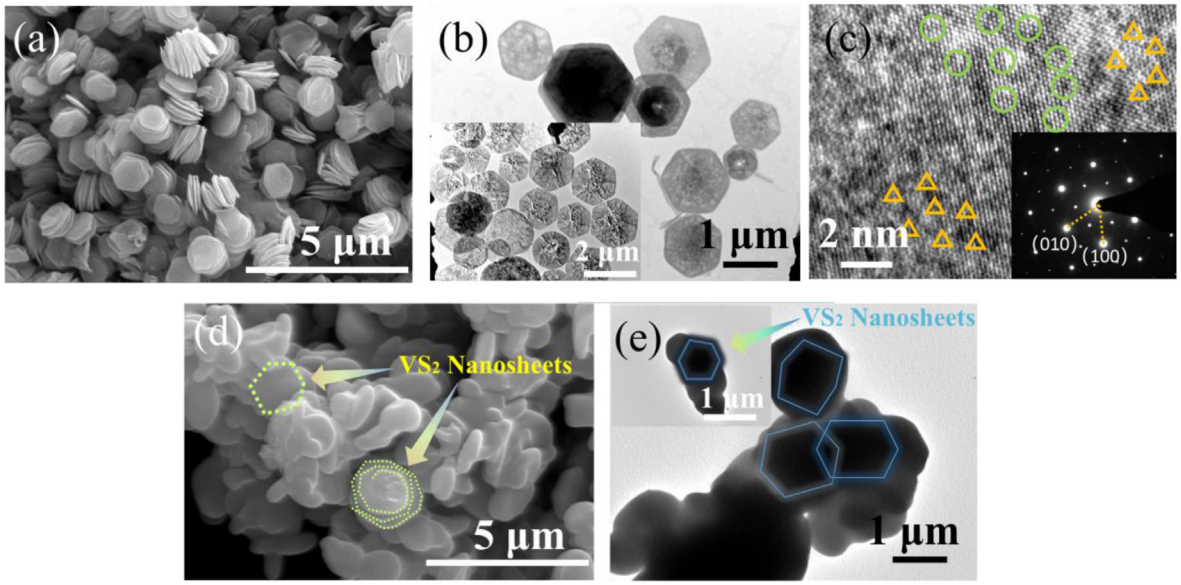

Fig. 3. (a) SEM images and (b) TEM images of VS_2 nanosheets; (c) HR-TEM images of VS_2 nanosheets (The inset is a SADE image); (d) SEM images and (e) TEM images of VS_2/GDC hybrids.

$$\varepsilon\prime = \varepsilon_\infty + \frac{\varepsilon_s - \varepsilon_\infty}{1+\omega^2\tau^2}, \tag{4}$$

$$\varepsilon'' = \frac{\varepsilon_s - \varepsilon_\infty}{1+\omega^2\tau^2}\omega\tau + \frac{\sigma}{\omega\varepsilon_0}, \tag{5}$$

where ε_∞ is the relative dielectric constant at infinite frequency, ε_s is the static permittivity, ω is the angular frequency, τ is the polarization relaxation time, σ is the electrical conductivity, and ε_0 ($\varepsilon_0 = 8.854 \times 10^{-12}$ F/m) is the vacuum dielectric constant. Generally, the relationship between ϵ' and ϵ" can be inferred as follow:

$$\left(\varepsilon\prime - \frac{\varepsilon_s + \varepsilon_\infty}{2}\right) + \varepsilon''^2 = \left(\frac{\varepsilon_s - \varepsilon_\infty}{2}\right)^2, \tag{6}$$

Fig. 4 displays the frequency-dependent ε', ε" and tanδ_ε for VS_2, GDC-700 °C, VS_2/GDC-700 °C hybrids at 2–18 GHz. As shown in Fig. 4, ε' and ε" decrease with increasing frequency, which could be caused by the increases ω due to the polarization relaxation in the low-frequency range. Compared with that of VS_2, ε' of VS_2/GDC-700 °C hybrids fluctuates with a slight decrease, while ε' is decreased by a large margin with increasing content of GDC-700 °C and is generally higher than that of GDC, as shown in Fig. 4a. As shown in Fig. 4, GDC encapsulates the surface of VS_2, where GDC has a low value of ϵ' and VS_2 has a high value of ϵ'. As a consequence, higher values of ϵ' for the hybrids could be inhibited with increasing amount of GDC added in the hybrids. Such effect of GDC on ϵ' of hybrids is more significant when the amount of GDC is high. As shown in Fig. 4b, VS_2, VS_2/10GDC-700 °C and VS_2/15GDC-700 °C have significantly higher ε" values than GDC-700 °C and VS_2/20GDC-700 °C, which are strongly dependent on the amount of GDC. It is known that ϵ" is determined by the relaxation loss and conductivity. The excessive doping of GDC leads to a large increase in the conductivity of the hybrid, which is not conducive to the effective absorption of EMW since high conductivity of system could cause the reflection of incident EMWs into free space. On the contrary, a moderate amount of GDC provides numerous conductivity paths for electrons hopping, enhancing the conductive loss. Furthermore, a large number of defects on the surface of GDC in VS_2/15GDC-700 °C will promote the interfacial polarization, relaxation loss and scattering response, which facilitate the dipole polarization. Clearly, as shown in Fig. 4c, tanδ_ε of VS_2/15GDC-700 °C is the highest among the samples, suggesting that the introduction of GDC in the hybrid would enhance the dielectric loss of VS_2/15GDC-700 °C. In addition, multiple interfacial polarizations in VS_2/15GDC-700 °C are beneficial for the enhanced EMW absorption performance. As described by equation (6), the plots of ε' versus ε" should be a semicircle corresponding to a Debye relaxation process, which is called the Cole-Cole semicircle. The Cole-Cole semicircles for all samples are shown in Fig. 4d. The VS_2, VS_2/10GDC-700 °C and VS_2/15GDC-700 °C samples show the semicircles in larger ranges of the plots than GDC-700 °C and VS_2/20GDC-700 °C samples, which could correspond to more significant polarization relaxation in the samples. The results demonstrate that the appropriate amount of GDC can promote the occurrence of multiple relaxation processes in the samples. When the content of GDC is increased, the EM attenuation mechanism of the pristine VS_2 nanosheets could be gradually changed from dipole polarization to conductive loss in the VS_2/GDC hybrids, confirming our view that the conductive loss is an essential factor in improving the EMW absorption performance.

The impedance matching (M_Z) and attenuation constant (α) are two important parameters that determine the EMW absorption performance of absorbers. To achieve zero reflection on the absorbers' surfaces, the characteristic impedance of the absorbers needs to be equal or close to that of the free space. The degree of impedance matching can be validated by the measure of M_Z, as follows [36,37]:

$$M_Z = \frac{2Z'_{in}}{|Z_{in}|^2 + 1}, \tag{7}$$

where Z' is the real part of normalized input impedance. In ordinary circumstances, the value of M_Z tends to be close to 1 for the absorbers with good impedance matching, which means that the incident EMW enters into the absorber as much as possible. The second important factor that measures the EMW absorption performance of absorbers is the attenuation constant α, which can be expressed by the following equation [38,39]:

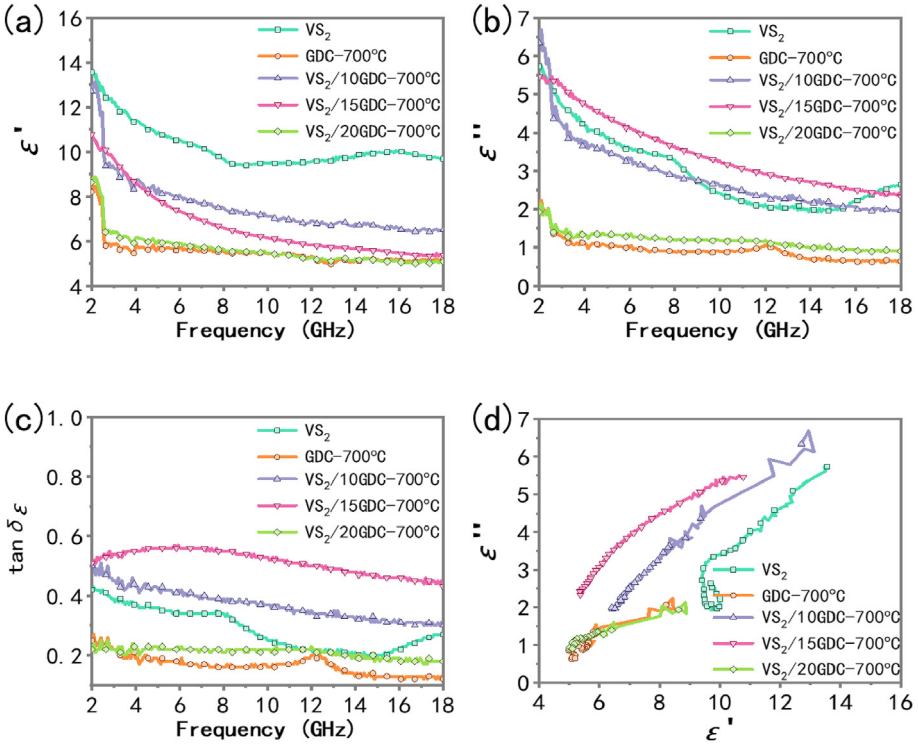

Fig. 4. (a) ε', (b) ε'', (c) $\tan\delta_\varepsilon$ and (d) Cole-Cole plots of VS_2, GDC and VS_2/GDC hybrids.

$$\alpha = \frac{\sqrt{2}\pi f}{c} \times \sqrt{(\mu'\varepsilon' - \mu'\varepsilon') + \sqrt{(\mu'\varepsilon' - \mu'\varepsilon')^2 + (\varepsilon'\mu' + \varepsilon'\mu')^2}}, \tag{8}$$

The electromagnetic attenuation capacity of the absorbers is determined by the conductive loss, dielectric loss and relaxation loss. The higher the value of α, the stronger the ability to attenuate the EMW inside the absorbers.

Fig. 5 shows R, M_Z, α and the contour map for the corresponding

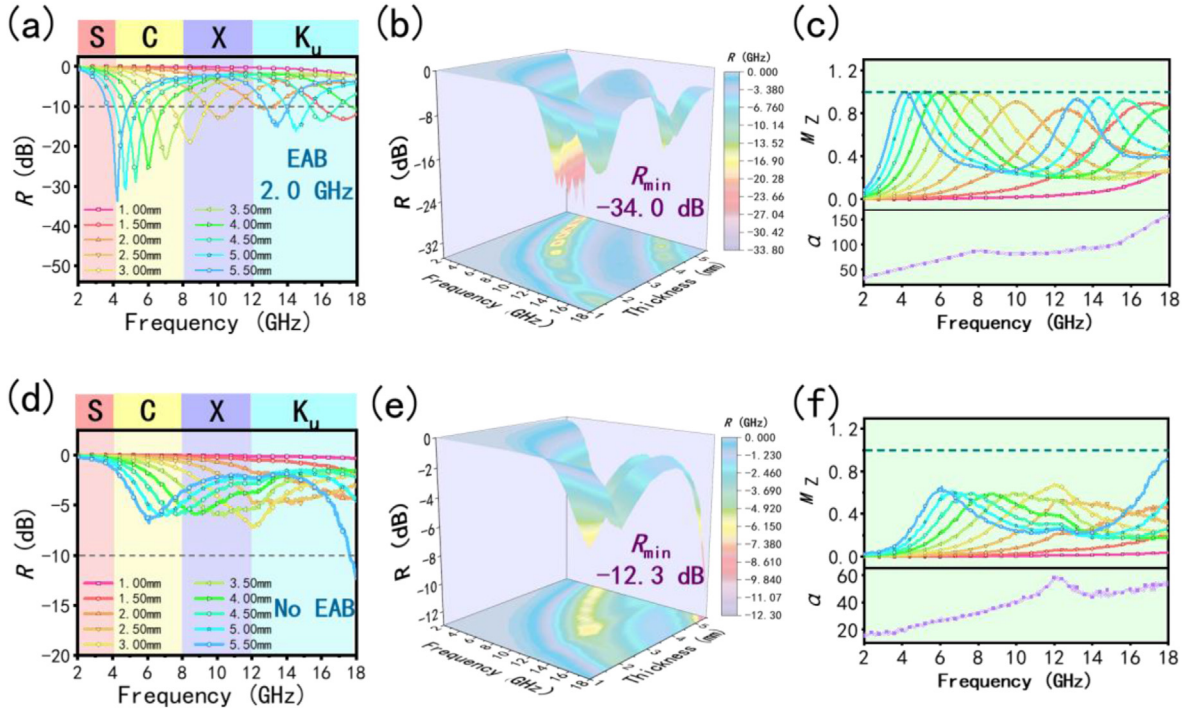

Fig. 5. (a) R, (b) contour map for the corresponding 3D R plots, (c) M_Z and α of VS_2; The (d) R, (e) contour map for the corresponding 3D R plots, (f) M_Z and α of GDC-700 °C.

3D R plots for VS_2 and GDC. As shown in Fig. 5a-c, R_{min} of VS_2 is about −34.0 dB with a thickness of 5.50 mm at a lower frequency of 4.2 GHz, which has an effective bandwidth of 2.0 GHz at a thickness of 3.0 mm. At the same time, M_Z with a thickness of 5.50 mm is also much close to 1 corresponding to the value of R_{min}, and α reaches the maximum value (α_{max}) of 155.5. The VS_2 sample with better EMW absorption performance has a thicker thickness and narrower effective bandwidth due to its low conductivity and sole absorption mechanism. To improve the EMW absorption performance of VS_2, GDC is introduced into VS_2 to improve its conductivity loss and dielectric loss. In order to analyze the changes in the absorbers before and after the addition of GDC, GDC-700 °C is chosen as a reference in comparative studies. As shown in Fig. 5d-f, GDC-700 °C at all thicknesses except for 5.50 mm do not show effective EMW absorption. The R_{min} value of GDC-700 °C is −12.3 dB at a thickness of 5.50 mm at 18.0 GHz corresponding to the M_Z value lower than 1, and the α_{max} value is 58.3. The GDC-700 °C exhibits the worst EMW absorption performance, which is attributed to the high electrical conductivity of the single carbon component that causes the reflection of most of the incident EMWs into free space, and a small amount of EMWs entering the absorber cannot be absorbed effectively.

As shown in Fig. 6a-c, with the introduction of 10 mL glucose, the EMW absorption performance of VS_2/10GDC-700 °C has been slightly improved. Compared to that of VS_2, the R_{min} value of VS_2/10GDC-700 °C reaches −37.4 dB at 4.9 GHz, which has an EAB of 3.7 GHz at a thickness of 2.0 mm. However, there is no obvious fluctuation in thickness and frequency band, suggesting that the addition of GDC with a low content does not influence the EMW absorption system. When the content of glucose reaches 15 mL in the system, VS_2/15GDC-700 °C shows excellent EMW absorption performance with almost all sample thicknesses, as shown in Fig. 6d-f. When M_Z is close to 1, αmax reaches 187.2, which proves that VS_2/15GDC-700 °C has good impedance matching and strong EM attenuation. The R_{min} value of VS_2/15GDC-700 °C is −34.4 dB with a thickness of 2.50 mm at a higher frequency of 13.3 GHz, which has an EAB of 5.7 GHz at a thickness of 2.5 mm. The results thus demonstrate that appropriate amount of GDC is effective in adjusting the impedance matching of the absorber and improving the attenuation of EMWs, especially in regulating the thickness and frequency band of the hybrid. In order to further explore the EMW absorption performance of VS_2/15GDC-700 °C, the EMW absorption performance of VS_2/15GDC-700 °C with a thickness of 2.50–2.95 mm is analyzed in detail, as shown in Fig. 6j-k. The R_{min} value of VS_2/15GDC-700 °C reaches −52.8 dB with a thickness of 2.70 mm at 12.2 GHz. It can be observed that VS_2/15GDC-700 °C achieves the best EMW absorption performance that could be ascribed to the synergistic effect of various factors. The multi-

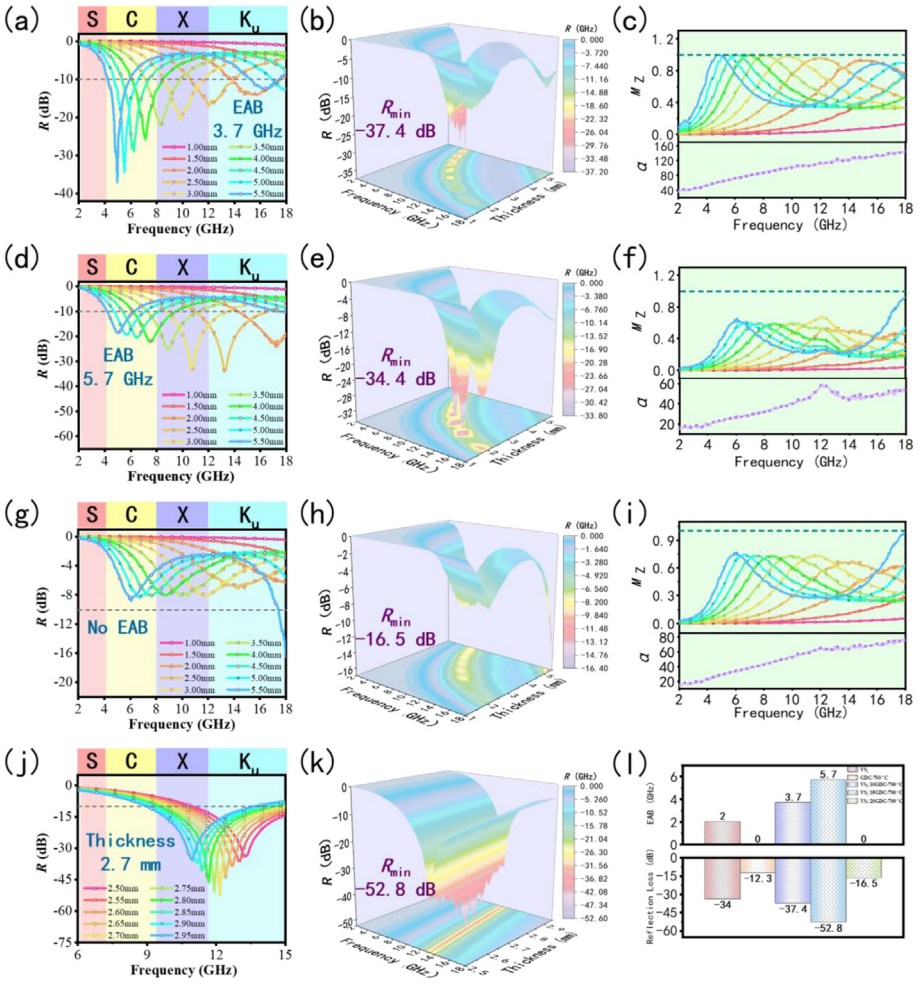

Fig. 6. (a) R, (b) contour map for the corresponding 3D R plots, (c) M_Z and α of VS_2/10GDC-700 °C; (d) R, (e) contour map for the corresponding 3D R plots, (f) M_Z and α of VS_2/15GDC-700 °C; (g) R, (h) contour map for the corresponding 3D R plots, (i) M_Z and α of VS_2/20GDC-700 °C; (j) R, (k) contour map for the corresponding 3D R plots of VS_2/15GDC-700 °C with a thickness of 2.50–2.95 mm; (l) EAB and R_{min} of VS_2, GDC-700 °C, VS_2/10GDC-700 °C, VS_2/15GDC-700 °C, VS_2/20GDC-700 °C.

component EMW absorption mechanisms are also attributed to the multi-interface heterostructures of the system, which is conducive to the multiple reflection and scattering of EMWs. As shown in Fig. 6g-i, when the amount of glucose in the system is increased to 20 mL, the EMW absorption of VS_2/20GDC-700 °C decreases sharply, which is similar to that of GDC-700 °C. The VS_2/20GDC-700 °C sample can absorb EMWs effectively only with the thickness of 5.50 mm. Its R_{min} is about −16.5 dB at 18.0 GHz corresponding to the M_Z value with a thickness of 5.50 mm, and α_{max} does not exceed 75.7. When a large number of GDC with high conductivity are coated on the surface of VS_2, the good EMW absorption performance of VS_2 could be inhibited to exhibit a high value of α. Moreover, when the multi-interface structure of the coaxial stacking VS_2 is masked by the coating of GDC, the interfacial polarization and multiple reflection could be promoted. As a result, the highest values of EAB and R_{min} of VS_2/15GDC-700 °C demonstrate that excellent EMW absorption performance can be achieved by the synergistic effect of various factors that adjust the M_Z and α values of the systems with strong EMW absorption, wide bandwidth and thin thickness, as shown in Fig. 6l. The broadening of the EAB realizes the compatibility of the absorption frequency band of the VS_2/GDC hybrids, and the tunable frequency band promotes the applicability of the VS_2/GDC hybrids in the range of 2–18 GHz, enhancing the EMW absorption in different frequency bands in a targeted manner. Furthermore, the reduction of thickness can effectively control the thickness of EMW absorption coating, which is conducive to improving the value of the practical applications. Importantly, the intervention of biomass carbon-based materials facilitates the synthesis of lightweight EMW absorbing materials [40].

The EMW absorption mechanisms of VS_2/GDC hybrids are illustrated in Fig. 7. The VB-group VS_2 nanomaterials with GDC coating break the technical bottleneck of narrow EAB, enabling the VS_2/GDC hybrids to occupy light weight and excellent EM parameters for the continuously tunable frequencies, which are attributed to the synergistic effect of multiple loss mechanisms. First, the abundant active sites located at the edges of microstructures and inside the VS_2 nanomaterials promote the occurrence of dipole polarization under the alternating EM fields. Meanwhile, the GDC coating as obtained by high-temperature carbonization accelerates the construction of defect structures, which could enhance EMW absorption by coupling with the polarization loss. Second, lattice distortions and vacancies could occur in the microstructures of stacked VS_2 nanomaterials as prepared by a well-tuned synthesis route, providing abundant defects for the EMW attenuation and EM energy conversion. Third, the multi-interface heterostructures are constructed by virtue of the full encapsulation of VS_2 nanomaterials with GDC, which could result in the rearrangement of local charges between the VS_2 nanomaterials and GDC coating with different conductivities, and thus the interface polarization. Fourth, the intervention of GDC adjusts the conductivity of the EM attenuation system, which can not only optimize the impedance matching for the EMWs that enter the absorbers as much as possible, but also generate plenty of freely moving electrons hopping between different energy levels of VS_2/GDC heterostructures in the system, leading to the enhanced conductive loss [41,42]. Last but not least, the multi-interface VS_2/GDC heterostructure and uniform distribution of VS_2 nanosheets with hexagonal stacking structure can also provide multiple reflection and scattering sites for the EMW absorption, ensuring that the EMWs can be effectively absorbed. To sum up, the excellent EMW absorption performance of VS_2/GDC hybrids with strong absorption, wide EAB, thin thickness could be made possible by the synergistic effect of the above-discussed factors [43–45], which undoubtedly contribute to the in-depth understanding of EMW absorption mechanisms and the development of VB-group TMDs nanomaterials in the field of EMW absorption.

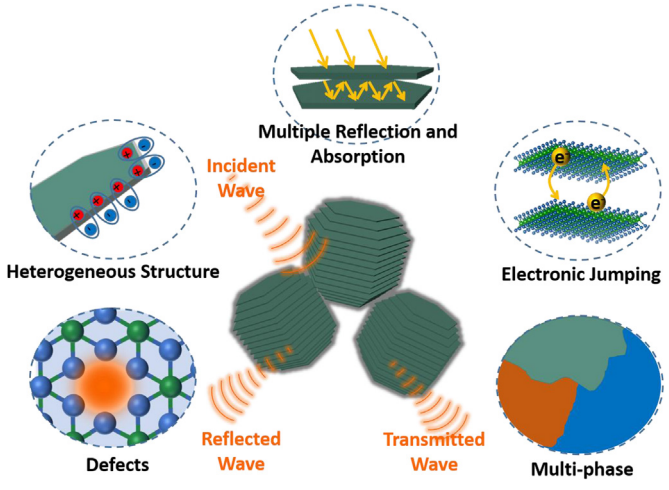

Fig. 7. Schematic illustration of the EMW absorption mechanisms in the VS_2/GDC hybrids.

4. Conclusions

In summary, the VS_2/GDC hybrids which exhibit the ameliorative EAB are successfully prepared by a facile hydrothermal method followed by high-temperature carbonization processes. The encapsulation of the stacked VS_2 nanomaterials by GDC can be modulated through controlling the doping amount of Glucose, optimizing the conductivity of the EMW absorption system and the construction of multi-interface VS_2/GDC heterostructures that are beneficial for the environmental stability and EMW absorption performance of the system. Because of the coupling effect of impedance matching and attenuation constant, the R_{min} value of VS_2/15GDC-700 °C is −52.8 dB with a thickness of 2.7 mm at a higher frequency of 12.2 GHz, which has an EAB of 5.7 GHz at a thickness of 2.5 mm, in comparison with those of pristine VS_2 nanomaterials. The coating of sugar-like biomass-derived GDC on the surface of stacked VS_2 nanosheets is assisted by the well-tuned microstructures of VS_2/GDC hybrids and defect engineering, which could enhance the conductive loss, dipole polarization, interface polarization, multiple reflections and scattering in the EMW absorbing materials. This work provides an in-depth understanding on the EMW absorption mechanisms of VB-group TMDs and opens a new avenue for the development of TMDs/biomass-based EMW absorbing materials with low cost, environmental friendliness and excellent EMW absorption performance.

Declaration of competing interest

The authors declare that they have no known competing financial interests or personal relationships that could have appeared to influence the work reported in this paper.

Acknowledgments

This work was supported by the National Natural Science Foundation of China (52102368, 52072192 and 51977009), Regional Joint Fund for Basic Research and Applied Basic Research of Guangdong Province (No. 2020SA001515110905).

Appendix A. Supplementary data

Supplementary data to this article can be found online at https://doi.org/10.1016/j.jmat.2022.12.003.

References

[1] Zhang D, Liu T, Shu J, Liang S, Wang X, Cheng J, Wang H, Cao M. Self-assembly construction of WS_2-rGO architecture with green EMI shielding. ACS Appl Mater Interfaces 2019;11:26807–16.

[2] Cheng J, Zhang H, Xiong Y, Gao L, Wen B, Raza H, Wang H, Zheng G, Zhang D, Zhang H. Construction of multiple interfaces and dielectric/magnetic heterostructures in electromagnetic wave absorbers with enhanced absorption performance: a review. Journal of Materiomics 2021;7:1233–63.

[3] Wu H, Liu J, Liang H, Zang D. Sandwich-like Fe_3O_4/Fe_3S_4 composites for electromagnetic wave absorption. Chem Eng J 2020;393:124743.

[4] Yang J, Wang J, Li H, Wu Z, Xing Y, Chen Y, Liu L. MoS_2/MXene aerogel with conformal heterogeneous interfaces tailored by atomic layer deposition for tunable microwave absorption. Adv Sci 2022;9:2101988.

[5] Liu L, Zhang S, Yan F, Li C, Zhu C, Zhang X, Chen Y. Three-dimensional hierarchical MoS_2 nanosheets/ultralong N-doped carbon nanotubes as high-performance electromagnetic wave absorbing material. ACS Appl Mater Interfaces 2018;10:14108–15.

[6] Sun X, Pu Y, Wu F, He J, Deng G, Song Z, Liu X, Shui J, Yu R. 0D-1D-2D multidimensionally assembled Co_9S_8/CNTs/MoS_2 composites for ultralight and broadband electromagnetic wave absorption. Chem Eng J 2021;423:130132.

[7] Zhang D, Liu T, Cheng J, Cao Q, Cao MS. Lightweight and high-performance microwave absorber based on 2D WS_2–RGO heterostructures. Nano-Micro Lett 2019;11:38.

[8] Zhang D, Wang H, Cheng J, Han C, Yang X, Xu J, Shan G, Zheng G, Cao M. Conductive WS_2-NS/CNTs hybrids based 3D ultra-thin mesh electromagnetic wave absorbers with excellent absorption performance. Appl Surf Sci 2020;528:147052.

[9] Kumar P, Verma NC, Goyal N, Biswas J, Lodha S, Nandi CK, Balakrishnan V. Phase engineering of seamless heterophase homojunctions with co-existing 3R and 2H phases in WS_2 monolayers. Nanoscale 2018;10:3320–30.

[10] Ding W, Hu L, Liu QC, Sheng ZG, Dai JM, Zhu XB, Sun YP. Structure modulation induced enhancement of microwave absorption in WS_2 nanosheets. Appl Phys Lett 2018;113:243102.

[11] Su J, Wang M, Li Y, Wang F, Chen Q, Luo P, Han J, Wang S, Li H, Zhai T. Sub-millimeter-scale monolayer p-type H-phase VS_2. Adv Funct Mater 2020;30:2000240.

[12] Zhang D, Zhang H, Cheng J, Raza H, Liu T, Liu B, Ba X, Zheng G, Chen G, Cao M. Customizing coaxial stacking VS_2 nanosheets for dual-band microwave absorption with superior performance in the C- and Ku-bands. J Mater Chem C 2020;8:5923–33.

[13] Zhang D, Liu T, Zhang M, Zhang H, Yang X, Cheng J, Shu J, Li L, Cao M. Confinedly growing and tailoring of Co_3O_4 clusters-WS_2 nanosheets for highly efficient microwave absorption. Nanotechnology 2020;31:325703.

[14] Liang L, Li Q, Yan X, Feng Y, Wang Y, Zhang HB, Zhou X, Liu C, Shen C, Xie X. Multifunctional magnetic $Ti_3C_2T_x$ MXene/graphene aerogel with superior electromagnetic wave absorption performance. ACS Nano 2021;15:6622–32.

[15] Cheng J, Zhang H, Wang H, Huang Z, Raza H, Hou C, Zheng G, Zhang D, Zheng Q, Che R. Tailoring self-polarization of bimetallic organic frameworks with multiple polar units toward high-performance consecutive multi-band electromagnetic wave absorption at Gigahertz. Adv Funct Mater 2022:2201129.

[16] Zhang D, Yang X, Cheng J, Lu M, Zhao B, Cao M. Facile preparation, characterization, and highly effective microwave absorption performance of CNTs/Fe_3O_4/PANI nanocomposites. J Nanomater 2013:591893.

[17] Li Q, Zhang Z, Qi L, Liao Q, Kang Z, Zhang Y. Toward the application of high frequency electromagnetic wave absorption by carbon nanostructures. Adv Sci 2019;6:1801057.

[18] Liu P, Gao S, Wang Y, Huang Y, He W, Huang W, Luo J. Carbon nanocages with N-doped carbon inner shell and Co/N-doped carbon outer shell as electromagnetic wave absorption materials. Chem Eng J 2020;381:122653.

[19] Zhang X, Qiao J, Jiang Y, Wang F, Tian X, Wang Z, Wu L, Liu W, Liu J. Carbon-based MOF derivatives: emerging efficient electromagnetic wave absorption agents. Nano-Micro Lett 2021;13:135.

[20] Liu N, Wang Y, Zhang X, He E, Zhang Z, Yu L. Litchi-like porous carbon nanospheres prepared from crosslinked polymer precursors for supercapacitors and electromagnetic wave absorption. Chem Eng J 2021;416:128926.

[21] Lyu L, Wang F, Li B, Zhang X, Qiao J, Yang Y, Liu J. Constructing 1T/2H MoS_2 nanosheets/3D carbon foam for high-performance electromagnetic wave absorption. J Colloid Interface Sci 2021;586:613–20.

[22] Zhang D, Xiong Y, Cheng J, Chai J, Liu T, Ba X, Ullah S, Zheng G, Yan M, Cao M. Synergetic dielectric loss and magnetic loss towards superior microwave absorption through hybridization of few-layer WS_2 nanosheets with NiO nanoparticles. Sci Bull 2020;65:138–46.

[23] Zhou X, Jia Z, Feng A, Wang K, Liu X, Chen L, Cao H, Wu G. Dependency of tunable electromagnetic wave absorption performance on morphology-controlled 3D porous carbon fabricated by biomass. Compos Commun 2020;21:100404.

[24] Zhou X, Jia Z, Feng A, Kou J, Cao H, Liu X, Wu G. Construction of multiple electromagnetic loss mechanism for enhanced electromagnetic absorption performance of fish scale-derived biomass absorber. Compos B Eng 2020;192:107980.

[25] Zhao H, Cheng Y, Lv H, Ji G, Du Y. A novel hierarchically porous magnetic carbon derived from biomass for strong lightweight microwave absorption. Carbon 2019;142:245–53.

[26] Liu T, Liu N, Gai L, An Q, Xiao Z, Zhai S, Cai W, Wang H, Li Z. Hierarchical carbonaceous composites with dispersed Co species prepared using the inherent nanostructural platform of biomass for enhanced microwave absorption. Microporous Mesoporous Mater 2020;302:110210.

[27] Guan H, Wang Q, Wu X, Pang J, Jiang Z, Chen G, Dong C, Wang L, Gong C. Biomass derived porous carbon (BPC) and their composites as lightweight and efficient microwave absorption materials. Compos B Eng 2021;207:108562.

[28] Dong S, Zhang W, Zhang X, Hu P, Han J. Designable synthesis of core-shell SiCw@C heterostructures with thickness-dependent electromagnetic wave absorption between the whole X-band and Ku-band. Chem Eng J 2018;354:767–76.

[29] Liu Z, Li N, Su C, Zhao H, Xu L, Yin Z, Li J, Du Y. Colloidal synthesis of 1T' phase dominated WS_2 towards endurable electrocatalysis. Nano Energy 2018;50:176–81.

[30] Qin M, Zhang L, Zhao X, Wu H. Defect induced polarization loss in multi-shelled spinel hollow spheres for electromagnetic wave absorption application. Adv Sci 2021;8:2004640.

[31] Lv H, Yang Z, Wang PL, Ji G, Song J, Zheng L, Zeng H, Xu ZJ. A voltage-boosting strategy enabling a low-frequency, flexible electromagnetic wave absorption device. Adv Mater 2018;30:1706343.

[32] Qin M, Zhang L, Zhao X, Wu H. Lightweight Ni foam-based ultra-broadband electromagnetic wave absorber. Adv Funct Mater 2021;31:2103436.

[33] Huang Y, Xie A, Seidi F, Zhu W, Li H, Yin S, Xu X, Xiao H. Core-shell heterostructured nanofibers consisting of Fe_7S_8 nanoparticles embedded into S-doped carbon nanoshells for superior electromagnetic wave absorption. Chem Eng J 2021;423:130307.

[34] Shu R, Li W, Wu Y, Zhang J, Zhang G. Nitrogen-doped Co-C/MWCNTs nanocomposites derived from bimetallic metal–organic frameworks for electromagnetic wave absorption in the X-band. Chem Eng J 2019;362:513–24.

[35] Zhang X, Huang Y, Liu P. Enhanced electromagnetic wave absorption properties of poly(3,4-ethylenedioxythiophene) nanofiber-decorated graphene sheets by non-covalent interactions. Nano-Micro Lett 2016;8:131–6.

[36] Liang C, Wang Z. Eggplant-derived SiC aerogels with high-performance electromagnetic wave absorption and thermal insulation properties. Chem Eng J 2019;373:598–605.

[37] Zhao G, Lv H, Zhou Y, Zheng X, Wu C, Xu C. Self-assembled sandwich-like MXene-derived nanocomposites for enhanced electromagnetic wave absorption. ACS Appl Mater Interfaces 2018;10:42925–32.

[38] Ding Y, Zhang Z, Luo B, Liao Q, Liu S, Liu Y, Zhang Y. Investigation on the broadband electromagnetic wave absorption properties and mechanism of Co_3O_4-nanosheets/reduced-graphene-oxide composite. Nano Res 2017;10:980–90.

[39] Ma L, Hamidinejad M, Liang C, Zhao B, Habibpour S, Yu A, Filleter T, Park CB. Enhanced electromagnetic wave absorption performance of polymer/SiC-nanowire/MXene ($Ti_3C_2T_x$) composites. Carbon 2021;179:408–16.

[40] Yao L, Yang W, Zhou S, Mei H, Cheng L, Zhang L. Design paradigm for strong-lightweight perfect microwave absorbers: the case of 3D printed gyroid shellular SiOC-based metamaterials. Carbon 2022;196:961–71.

[41] Huang Z, Cheng J, Zhang H, Xiong Y, Zhou Z, Zheng Q, Zheng G, Zhang D, Cao M. High-performance microwave absorption enabled by Co_3O_4 modified VB-group laminated VS_2 with frequency modulation from S-band to Ku-band. J Mater Sci Technol 2022;107:155–64.

[42] Zhao Z, Zhang L, Wu H. Hydro/organo/ionogels: “controllable” electromagnetic wave absorbers. Adv Mater 2022;34:2205376.

[43] Liang H, Zhang L, Wu H. Exploration of twin-modified grain boundary engineering in metallic copper predominated electromagnetic wave absorber. Small 2022;18:2203620.

[44] Cheng J, Zhang H, Ning M, Raza H, Zhang D, Zheng G, Zheng Q, Che R. Emerging materials and designs for low-and multi-band electromagnetic wave absorbers: the search for dielectric and magnetic synergy? Adv Funct Mater 2022:2200123.

[45] Bi Y, Ma M, Liao Z, Tong Z, Chen Y, Wang R, Ma Y, Wu G. One-dimensional Ni@Co/C@PPy composites for superior electromagnetic wave absorption. J Colloid Interface Sci 2022;605:483–92.

Honghan Wang received her B.E. degree and Master degree from Qiqihar University in 2018. Now she is a PhD student at Dalian Polytechnic University. Her current research interests focus on the development of metal disulfide hybrid absorbing materials by atom layer deposition route.

Junye Cheng received his Ph.D. degree from City University of Hong Kong in 2019. His current research interests focus on the development of 2D nanomaterials for applications in energy storage and conversion, environmental protection, as well as electromagnetic microwave absorption.

Deqing Zhang received his Ph.D. degree from Harbin Engineering University in 2006. Currently, he is Full Professor at Qiqihar University. His research interests include ferroelectric materials, piezoelectric ceramic materials, and 2D nanomaterials for applications in microwave absorption.

Shangru Zhai is Full Professor at Dalian Polytechnic University. His research interests include developing biomass-based materials, porous material and other environmental functional materials.

Mao-Sheng Cao received his B.S. degree from Heilongjiang University in 1983, and his M.S. and Ph.D. degrees from Harbin Institute of Technology in 1989 and 1998, respectively. He is a distinguished professor at the Beijing Institute of Technology. His research interest includes electromagnetic functional materials and devices.